Results in Physics 17 (2020) 103051

Contents lists available at ScienceDirect

Results in Physics

journal homepage: www.elsevier.com/locate/rinp

A comparative study of the mechanical integrity of natural hydroxyapatite scaffolds prepared from two biogenic sources using a low compaction pressure method

E.S. Akpan[a], M. Dauda[a], L.S. Kuburi[a], D.O. Obada[a,d,*], D. Dodoo-Arhin[b,c,*]

[a] Department of Mechanical Engineering, Ahmadu Bello University, Zaria, Nigeria
[b] Department of Materials Science and Engineering, University of Ghana, Legon, Ghana
[c] Institute of Applied Science and Technology, University of Ghana, Legon, Ghana
[d] Africa Center of Excellence on New Pedagogies in Engineering Education, Ahmadu Bello University, Zaria, Nigeria

ARTICLE INFO

Keywords:
Sintering
Mechanical properties
Apatite
Bone implants
Ca/P molar ratio

ABSTRACT

With a view to enhancing laboratory and application-based pedagogical approaches in bioengineering, a comparison of the physical, chemical and mechanical properties of natural hydroxyapatite produced from non-separated animal bones (NB) and catfish bones (CB) obtained by thermal treatment and a low compaction pressure method has been reported in this study. The structure, morphology and surface chemistry of the processed biomaterials were characterized by X-ray diffraction (XRD), scanning electron microscopy (SEM) and infrared spectroscopy, respectively. Uniaxial compaction using a pressure of 1 MPa was used on circular shaped hydroxyapatite scaffolds to measure the mechanical properties of the produced scaffolds. From XRD analysis, both samples showed prominent reflections of the hydroxyapatite phase, suggesting high crystallinity and phase stability. The morphology of the powders showed irregular shapes with large agglomerates for non-separated animal bones-derived hydroxyapatite as compared to more open pores in the catfish bones-derived hydroxyapatite. Hydroxyapatite produced from catfish bones revealed a microstructure with open pores which is useful in terms of cell adhesion. The hydroxyapatite products revealed Ca/P ratios of 1.58 and 1.63 for catfish bones (CB) and non-separated animal bones-derived hydroxyapatite, respectively. Improvements in the fracture toughness were observed for CB in comparison with NB. Calculated fracture toughness values were 5.72 MPa. $m^{1/2}$ and 2.35 MPa. $m^{1/2}$ for catfish bones and non-separated animal bones-derived scaffold respectively. These results are useful in terms of the production and biomedical applications of natural hydroxyapatite.

Introduction

It is well known that the production of hydroxyapatite (HAp) has consistently been processed from natural sources such as animal bones [1], fish bone [2], coral [3], and egg shells [4–6]. Hydroxyapatite from natural sources is preferable as compared to the synthetic type for biomedical applications [7]. This is because natural HAp has, in trace amounts, magnesium, potassium, strontium and sodium inherent in its chemical structure. Hydroxyapatite (HAp) by virtue of its unique characteristics is quite useful as medical implants and hard tissue replacement by virtue of its huge similarity with hard tissue of human bones and teeth [8–10].

Nonetheless, the use of HAp is hampered mechanically by virtue of its low fracture toughness, making it liable to failure [11]. The low mechanical integrity may be linked to heat treatment which initiates and allow the propagation of rough grained morphology, resulting in poor mechanical characteristics. Mechanical properties evaluation and dataset is very important to ascertain the mechanical integrity of developed hydroxyapatite scaffolds. A plethora of studies to ascertain the mechanical characteristics of hydroxyapatite scaffolds is available in the literature [1,12–18], while there are inadequate mechanical property datasets that reveal comparisons for apatites produced from different natural sources.

The brittleness of bio-ceramic has over time limited their applications in biomedicine as they exhibit strength when subjected to compressive forces but quite weak under tensile and shear forces. It is possible to enhance the mechanical properties of HAp by preparing the scaffolds with relatively high compaction pressure. This protocol has

* Corresponding authors at: Department of Mechanical Engineering, Ahmadu Bello University, Zaria, Nigeria (D.O. Obada). Department of Materials Science and Engineering, University of Ghana, Legon, Ghana (D. Dodoo-Arhin).
E-mail addresses: doobada@abu.edu.ng (D.O. Obada), ddodoo-arhin@ug.edu.gh (D. Dodoo-Arhin).

https://doi.org/10.1016/j.rinp.2020.103051
Received 15 December 2019; Received in revised form 4 March 2020; Accepted 4 March 2020
Available online 07 March 2020

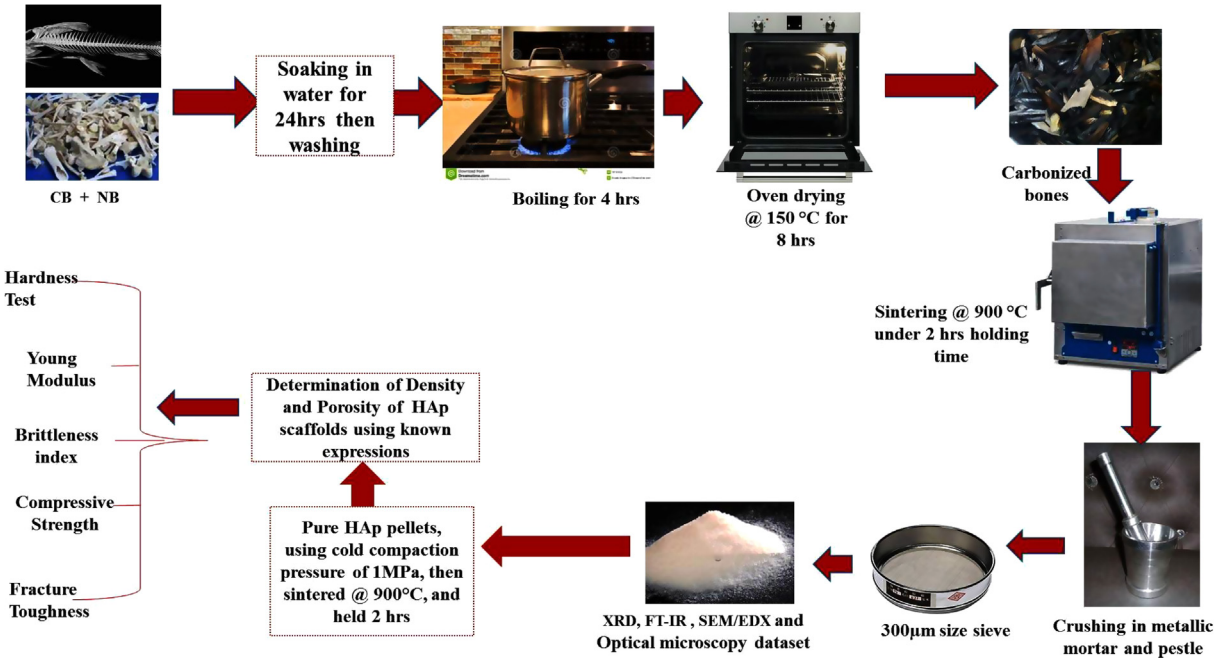

Fig. 1. Methodological protocol for the synthesis and characterization of produced HAp.

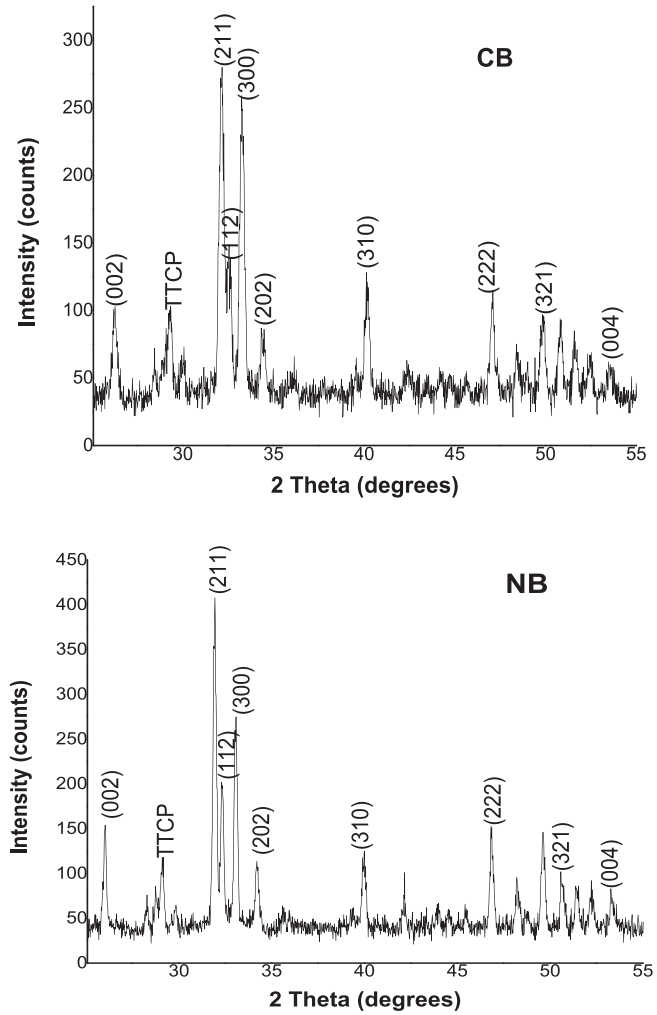

Fig. 2. X-ray diffraction patterns for the synthesized CB and NB-derived hydroxyapatite and identification of the HAp lattice planes.

conformed to progress made in the fabrication of bioceramics. As per process parameters, to produce pure and clinically required hydroxyapatite, one facile method of producing hydroxyapatite scaffolds is cold isostatic pressing. In this way, sintering after shaping of green ceramic compacts has been done [1,19,20]. In order to improve the homogeneity in densification and microstructure, cold pressing is viable by virtue of its isotropic pressure. In addition, this protocol has been used to manufacture biomaterials derived scaffolds and powders with fewer pores [21]. Stemming from these, studies have reported a reduction in compressive strength when compaction pressure is applied. This is possible because of the stress fields induced in the HAp powders during compaction which has the tendency to make it more susceptible to cracks. In a recent study by our group [1,20], very low cold compaction pressure (500 Pa) was proposed for compacting HAp powders, and this produced promising mechanical properties to a large extent due to reduced stress fields during powder compaction.

Here, we report a comparison of the physical, chemical and with more emphasis, the mechanical characteristics of hydroxyapatite produced from non-separated animal bones and catfish bones. The mechanical properties of the sintered bioceramics scaffolds assisted by low cold compaction pressure were presented and discussed.

Materials and method

Production of HAp powder from non-separated biowastes and catfish bones

Non-separated animal bones which are regarded as wastes were obtained from an abattoir in Zaria, Nigeria, while the catfish bones were sourced from restaurants, since they were tagged as wastes as well, in Zaria metropolis. The sourced bones (raw materials) were used as precursors for hydroxyapatite production. The non-separated animal bones were thoroughly cleaned and a detailed procedure can be found in studies by our group [1,20]. This procedure was used to clean/deproteinize the catfish bones as well. Tap water was used for cleaning the bones throughout the process. The cleaned bones were burnt by a flame in open air and subjected to sintering at 900 °C for 2 h at a heating rate of 5 °C/min. The sintered powdery hydroxyapatite samples sourced from the non-separated and catfish bones were labelled as NB and CB, respectively. These sample nomenclature were adopted in this study.

Table 1
Cell parameters of HAp derived from the biowaste bones.

Calcination temperature (°C)	Sample Code	Average crystallite size (nm)	Crystallinity (%)	c/a ratio
900	CB	37.2	99	0.79
900	NB	99	86.15	0.52

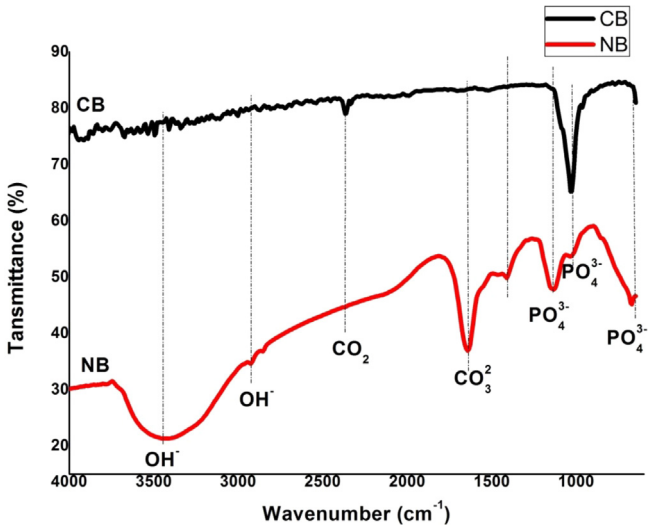

Fig. 3. FT-IR spectra for the synthesized CB and NB derived hydroxyapatites.

After sintering, the obtained HAp powders were milled in a metallic mortar and passed through a sieve of 300 μm mesh prior to powder analyses. The methodological approach for the processing, physical and mechanical properties measurement of the synthesized HAp is as shown in Fig. 1. (Note: CB and NB were separately processed following the methodological sequence).

Chemical characterization of produced hydroxyapatite

X-ray diffraction (XRD) analysis

To investigate the structure and phases present in the synthesized HAp powders (NB and CB), diffraction patterns were collected on a Rigaku Miniflex diffractometer and powder crystallinity was calculated as expressed in Eq. (1) [22]:

$$x_c = 100 \times \frac{I_{300} - V_{112/300}}{I_{300}} \quad (1)$$

where I_{300} represents the intensity of (3 0 0) diffraction peak, $V_{112/300}$ represents the reflection of the hollow between (1 1 2) and (3 0 0) diffraction peaks of HAp. Identification of phases was done by comparing the diffraction patterns of HAp with JCPDS standards

Fourier transform infrared (FT-IR) analysis

Surface chemistry data was collected on a Fourier Transform Infrared Spectrometer at a resolution of four wavenumbers, operating from 4000 to 400 cm^{-1}.

Scanning electron microscopy (SEM) and energy dispersive X-Ray spectroscopy (EDX) analysis

The microstructure of the samples was studied on a Phenom ProX Desktop scanning electron microscope (SEM) equipped with EDX for elemental mapping and operated at 15 kV. Each sample was viewed at low magnifications of 300 and 500 xk. The EDX maps indicated the atomic and weight percentages of each element analyzed from obtained HAp. To view the samples at higher magnification, images were taken at 5000× using a JEOL JSM-7600F scanning electron microscope operated at 15 kV.

Optical microscopy

Optical microscopy images obtained using an optical microscope ((ICC50, DM 750, Leica, Wetzlar, Germany) was used to reveal some inherent structure of the produced apatites.

Physical characterization of produced hydroxyapatite

The physical characterization was split into two levels; measurement of porosity and the bulk powder densities

Porosity measurements

Porosity measurements of the produced hydroxyapatite were conducted using the expression from Eq. (2):

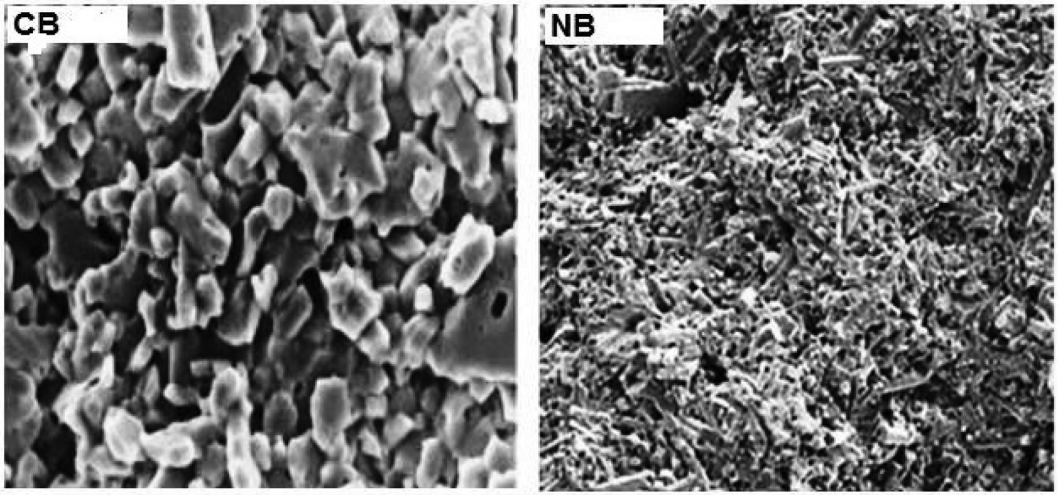

Fig. 4. Scanning electron micrographs of CB and NB-derived hydroxyapatite at high magnification (×5000).

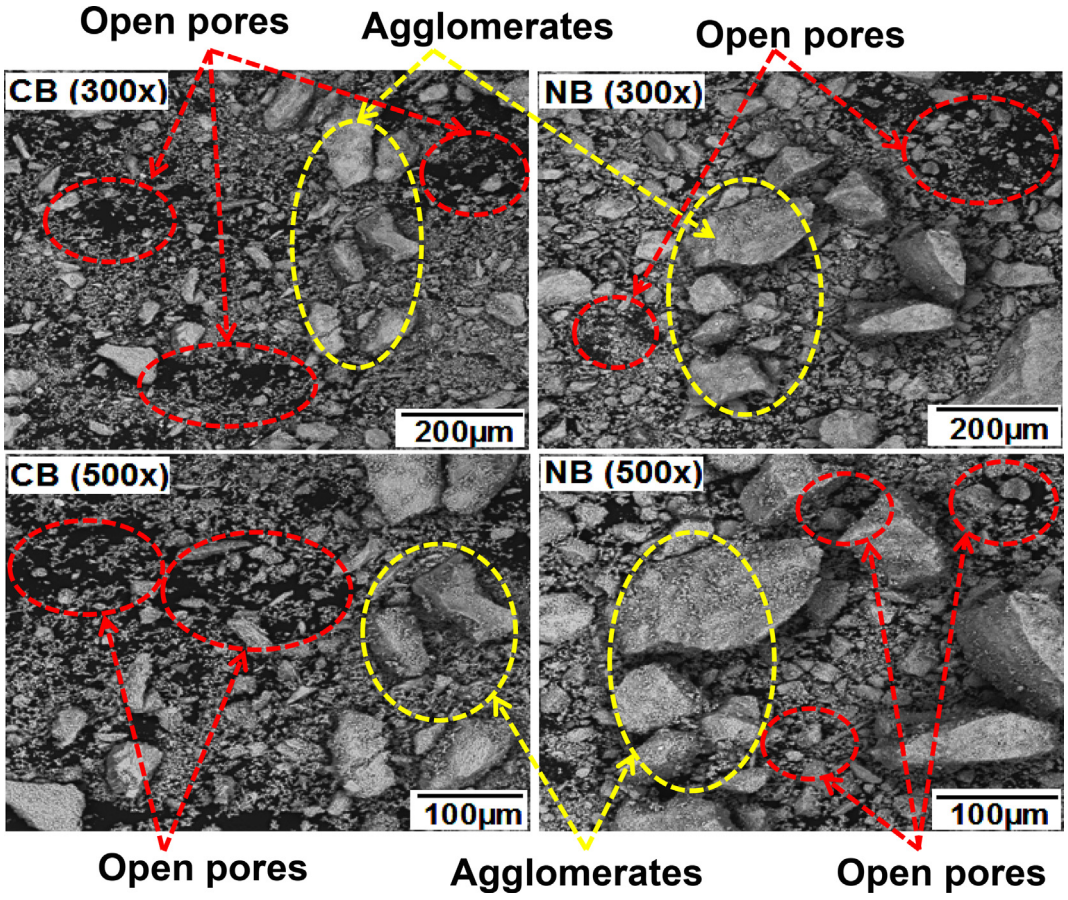

Fig. 5. Scanning electron micrographs of CB and NB-derived hydroxyapatite.

$$\text{Porosity}(\%) = \left(1 - \frac{\text{Weight of HAp}}{\text{Volume of HAp} \times \text{Density of HAp}}\right) \times 100 \quad (2)$$

The density of HAp used is the typical density of HAp (3.16 g/cm^3) [1,23–25].

Density measurements

The apparent densities of the produced hydroxyapatite were calculated from the dry weight and volume of the powders using the expression from Eq. (3):

$$\text{Apparent Density of HAp} = \frac{\text{Dry weight of HAp}}{\text{Volume filled by HAp}} \quad (3)$$

Mechanical testing

The powders were uniaxially pressed using a cold compaction pressure of 1 MPa in a 25 mm diameter cylindrical die. The produced green compacts were sintered in air atmosphere at 900 °C for a 2 h dwell time and at a heating and cooling rate of 5 °C/min.

The mechanical properties measurement conducted for the fabricated scaffolds were hardness, compression strength, elastic modulus, yield strength, fracture toughness and brittleness index. The details of all mechanical evaluations are reported elsewhere [1].

Results and discussion

XRD diffraction analysis

The XRD patterns for the synthesized CB and NB derived HAp are presented in Fig. 2. The major reflections matched those in the JCPDS card number 09-0432, which contains sharp and prominent reflections due to the high degree of crystallinity of the powders. The estimated degree of crystallinity was around 99.9% and 86.15% for CB and NB, respectively, while the mean crystallite size of CB and NB taken from $2\theta = 31.72^\circ$ (211 plane) was 37.1 nm and 99 nm, respectively. The higher degree of crystallinity for CB means the derived hydroxyapatite is more stable as compared to NB. Sintering the powdery hydroxyapatite precursors resulted in degradation of the hydroxyapatite phase to form small amounts of tetra-calcium phosphate (TTCP). The presence of TTCP may not be detrimental since this phase is biocompatible and has a high degree of solubility than hydroxyapatite [42].

Table 1 shows the crystallinity, crystallite size and cell parameters of the heat treated hydroxyapatite sourced from the biowastes which were estimated from the X-ray diffraction data. The variations observed in the crystallinity of the samples can be attributed to the gradient in molecular positioning during heat treatment. However, considerable crystallinity was recorded for the samples. The crystallite sizes show an inverse relationship as compared to the crystallinity of samples. For CB with comparative small crystallite size (37.2 nm), the crystallinity is higher and for NB with a large crystallite size (99 nm) the crystallinity is comparatively smaller. It means that the crystallite size is not dependent on crystallinity and a small crystallite size can cause the broadening of the XRD peaks as observed on the XRD patterns for CB (see Fig. 1). The values of the lattice parameters ratio (c/a) obtained in this study are close to values obtained in a study carried out by Pal et al. [41].

Surface chemistry

The FT-IR spectra obtained from the CB and NB powders (Fig. 3)

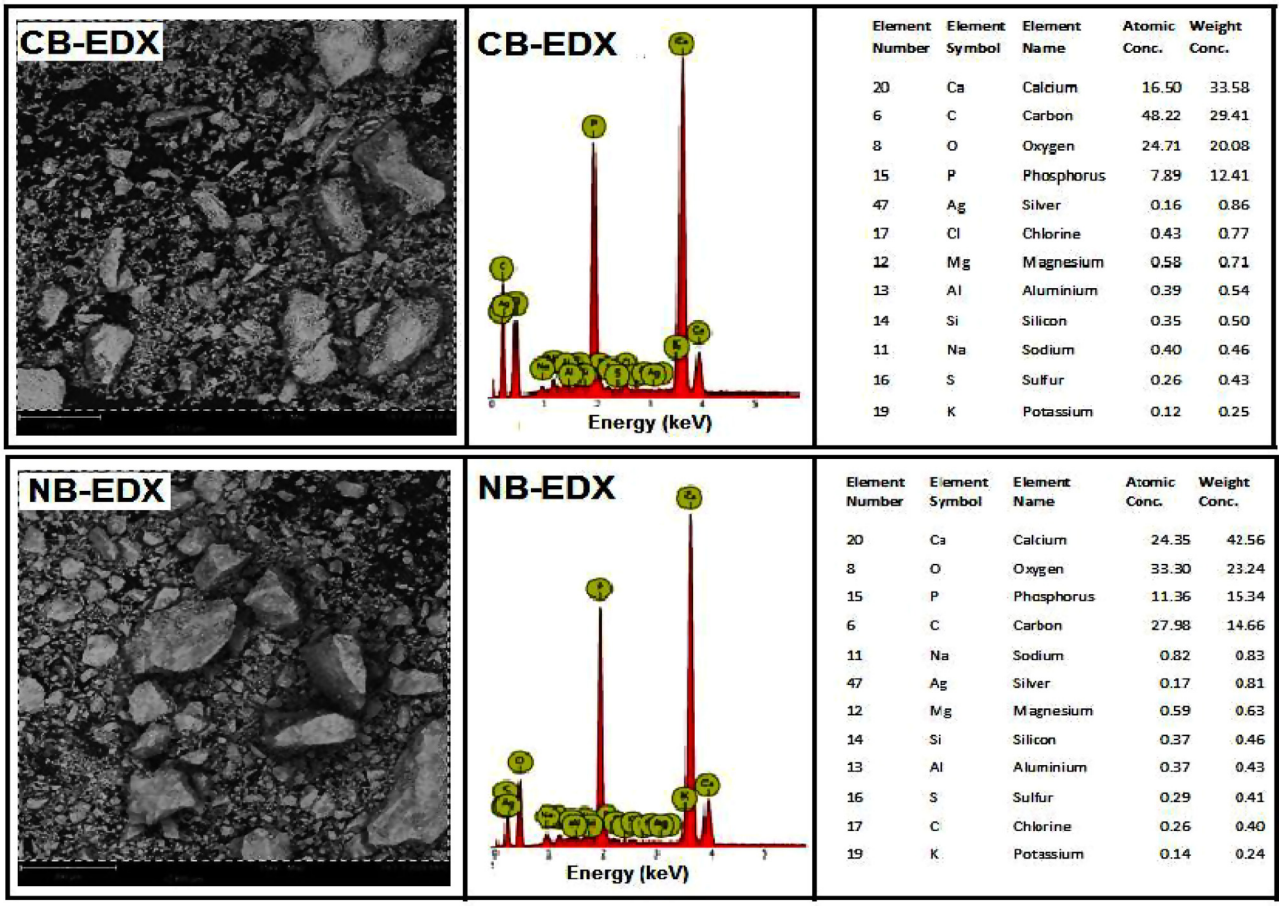

Element Number	Element Symbol	Element Name	Atomic Conc.	Weight Conc.
20	Ca	Calcium	16.50	33.58
6	C	Carbon	48.22	29.41
8	O	Oxygen	24.71	20.08
15	P	Phosphorus	7.89	12.41
47	Ag	Silver	0.16	0.86
17	Cl	Chlorine	0.43	0.77
12	Mg	Magnesium	0.58	0.71
13	Al	Aluminium	0.39	0.54
14	Si	Silicon	0.35	0.50
11	Na	Sodium	0.40	0.46
16	S	Sulfur	0.26	0.43
19	K	Potassium	0.12	0.25

Element Number	Element Symbol	Element Name	Atomic Conc.	Weight Conc.
20	Ca	Calcium	24.35	42.56
8	O	Oxygen	33.30	23.24
15	P	Phosphorus	11.36	15.34
6	C	Carbon	27.98	14.66
11	Na	Sodium	0.82	0.83
47	Ag	Silver	0.17	0.81
12	Mg	Magnesium	0.59	0.63
14	Si	Silicon	0.37	0.46
13	Al	Aluminium	0.37	0.43
16	S	Sulfur	0.29	0.41
17	C	Chlorine	0.26	0.40
19	K	Potassium	0.14	0.24

Fig. 6. EDX spectra of CB and NB derived hydroxyapatite.

exhibited a range of bands from 1100 ± 1550 cm^{-1} in addition to the peaks expected for hydroxyapatite (i.e. those related to the PO_4^{3-} and OH^- groups). Despite subjecting both HAp powders (CB and NB) to similar processing protocol, there was a broad peak around 3417 cm^{-1} in the spectra for NB, demonstrating the presence of adsorbed water [20]. This broad band is attributed to the ν_3 and ν_1 stretching modes of water molecules [43]. In addition, the band observed at 3497 cm^{-1} indicates the characteristic of O–H stretching vibration of HAp [44]. Bands that are similar to those obtained in this study have also been observed in previous studies [43,45,46]. The inclusion of the bands of carbonate in NB is attibuted with the adsorption of non-structural carbonate on the surface of NB [47].

SEM/EDX analysis

The microstructure of CB and NB powders at high magnification is shown in Fig. 4. Typical flower-like microstructure which consists of flakes of petal-like orientation are visible for CB derived hydroxyapatite. Flower like HA morphology has been described as an efficient carrier for the delivery of drugs [48].Rod-shaped particles are evident for NB and this description is similar to reports elsewhere [49]. The orientation of the NB particles which are inter-connected with grain structures which are close, typically defines the initiation of a defined crystalline grain structure of hydroxyapatite.

SEM images at low magnifications, ×300 and ×500 for CB and NB is presented in Fig. 5 and the grain distribution and orientations are observed. As noticed, the surface of CB and NB is overly porous and there is non-uniformity in the particle size distribution. At both magnifications, the powders are irregular in shape with more agglomerates noticed for the NB powders and quite smaller pores are present. The CB and NB particles presented layered shapes typical of HAp [26]. These results are in tandem with the SEM results obtained by [27] and [28]. It is worth noting that the images revealed the appearance of more open pores in the bulk of CB with lesser agglomerated structure, hence, the pores became wider (larger). Micrographs for CB show interconnected (open) porosity, and linking the degree of pore connectivity to the apparent density (Table 1), there are some trends evident in the variation of micro pore size and morphology, with apparent density. As expected, the micro pore sizes were found to decrease with increasing apparent density. It is also noted that the micropores were isolated spherical pores, which were randomly distributed throughout the bioceramic space for CB and NB and located within the ceramic grains. The higher porosity of prepared CB as compared to NB (Table 1) can be advantageous for applications in biomedicine.

EDX analysis revealed the elemental composition and the corresponding Ca/P molar ratio of the HA powders as shown in Fig. 6. The main elements of CB and NB are calcium (Ca), phosphorus (P) and oxygen (O) with an average atomic Ca/P molar ratio of 1.58 and 1.63 for CB and NB respectively. The EDX analysis reveals that HA extracted from the produced hydroxyapatite (CB and NB) contains ions such as Na^+, Mg^{2+} etc. in trace amounts such as reported by [29] and [30]. Presence of these trace ions are advantageous for natural HAp. These trace ions have the potential to enhance the formative and regenerative processes in bone [31].

The Ca/P ratios of HAp obtained in this study has slight variations from the theoretical value for stoichiometric HAp of 1.67. One factor this variation is attributed to, is the processing (burning in open air), which may not have completely removed the fats and soft tissues and possibly have increased the elemental composition of carbon (C) in the resultant powders after sintering. Furthermore, the sintering

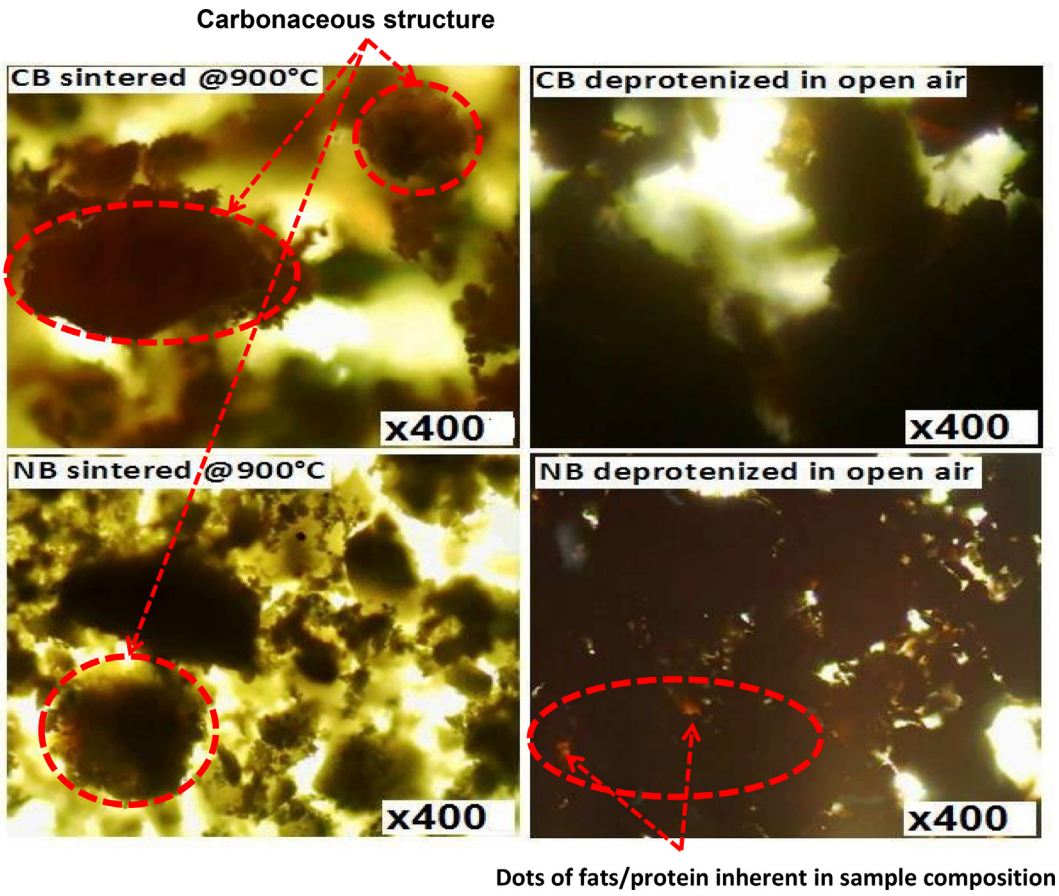

Fig. 7. Optical micrographs of NB and CB samples.

Table 2
The densities of CB and NB-derived hydroxyapatite.

Samples Notation	$\%D_1$	$\%D_2$	$\%D_3$	$\%D_{avg}$	SD
CB	1.63	1.60	1.62	1.62	0.01
NB	1.69	1.69	1.67	1.68	0.01

$\%\ D_{1\text{-}3}$ = Percentage densities of the 2 samples.
SD = Standard Deviation.

Table 3
The porosities of CB and NB-derived hydroxyapatite.

Samples notation	$\%P_1$	$\%P_2$	$\%P_3$	$\%P_{avg}$	SD
CB	48.4	49.2	48.7	48.8	0.33
NB	46.7	46.5	47.2	46.8	0.03

$\%\ P_{1\text{-}3}$ = Percentage porosities of the 2 samples.
SD = Standard Deviation.

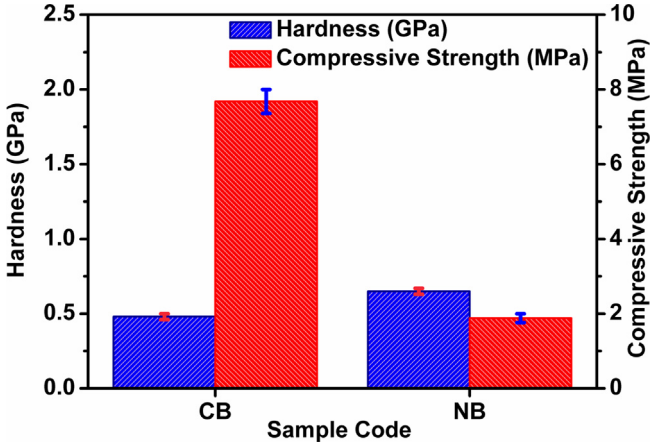

Fig. 8. Hardness and compressive strength values of CB and NB derived scaffolds.

temperature which influences the composition of compounds with inherent calcium could be another reason for this deviation as reported in studies elsewhere [29,32,33]. In similar vein, the high carbon content from EDX analysis can be attributed to high cholesterol and protein concentrations and the calcium hydroxyapatite rich areas. These results are similar to a study conducted by [34], where they inferred that cholesterol-rich areas of calcium hydroxyapatite showed higher signals for C and O and also, areas rich in calcium showed greater amounts of C, O, P, and Ca.

The optical microscopy images as shown in Fig. 7 were used to examine the passage of light through the powders in order to reveal its internal morphology. Optical microscopy observations show a texture which can be traced to the high carbon content observed in the EDX spectra of the produced HAp. The images for CB and NB show much diversified walls as per internal and external shapes and orientation. For the deproteinized CB and NB samples, dots of fats can be observed showing residual matter and this can also be observed for the sintered samples as well. This may have caused the high carbon content as revealed in the elemental composition (see Fig. 6) and the formation of three dimensional carbonaceous structures observed in the optical microstructures of the sintered samples.

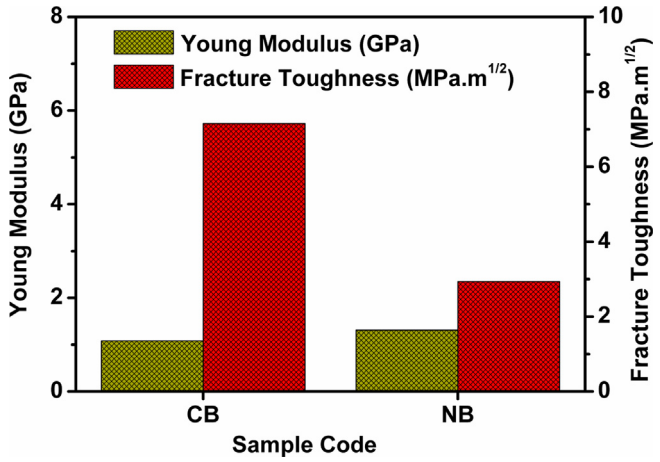

Fig. 9. Young modulus and fracture toughness values of CB and NB derived scaffolds.

Samples density and porosity measurements

Apparent density (Table 2) for CB and NB was found to range from 1.62 ± 0.01 and 1.68 ± 0.01 g/cm^3 respectively which depicts that NB is denser with less open porosity. Table 3 reveals the variations in porosity for CB and NB. The porosity of CB, 48.8 ± 0.33% is higher as compared to NB which was calculated as 46.8 ± 0.03%. It has been reported that porosities in the range of 40 to 90% encouraged osteointegration [1,35]. It is safe to say that the calculated porosities show potential of the suitability of CB and NB for biomedical applications. Stemming from this, CB has greater potential to be used for biomedical applications where higher porosity would be useful.

Mechanical measurements

The Vickers hardness and compression strength variation is shown in Fig. 8. Vickers hardness increased from a value of 0.48 GPa for CB to a value of 0.65 GPa for NB. The increase in hardness could be attributed to the increase in relative density as shown in Table 3. It is well known that the hardness of HAp scaffolds increase with increasing relative density [48]. The relative decrease in the Vickers hardness of CB can also be attributed to the decomposition of HAp phase [50,51] as confirmed by the formation of small amounts of tetra-calcium phosphate (TTCP) as shown in Fig. 2.The variation in compressive strength can be related to the calculated apparent densities of the samples with the compressive strength increasing from approximately 0.47 to 1.92 MPa for NB and CB respectively This advances the viability of CB in this regard for use in biomedical applications where compressive stresses is a common phenomenon, for instance, trabecular bone in the foot area. Hardness values for CB and NB are within the range reported for human femoral cortical bone [36], and this advances the usefulness of the synthesized products in biomedicine.

Fig. 9 show plots of the elastic modulus and fracture toughness of the produced scaffolds. Calculated fracture toughness value was 5.72 MPa. m$^{1/2}$ and 2.35 MPa. m$^{1/2}$ for CB and NB derived hydroxyapatite scaffold respectively. This decrease in the fracture toughness for NB is linked with the higher hardness value of NB and partially to the decomposition of the HA phase to TTCP. In the present work, the high toughness recorded (~5.72 MPa. m$^{1/2}$) while maintaining a stable phase at 900 °C is quite encouraging as many studies reported a much lower fracture toughness value (below 1.2 MPa. m$^{1/2}$) for their HAp [48,52–57].The overall mechanical properties of the synthesized HAp were in line with values obtained by other researchers [16,19,37–40]. Brittleness index for CB and NB were 0.084 and 0.277 respectively. Comparatively, the NB derived-scaffolds are more prone to cracks.

It can be emphasized, particularly for biomedical teams interested in the eventual application of these ceramics, that the compressive strength of CB was no higher than 2 MPa, a value that can be considered sufficient with room for improvement. Also, the main advantage of these produced bio-ceramics, beyond their capability of providing diversified architectures and a variety of pore size distribution, is the fact that they have satisfactory mechanical strength - allowing for use under less load bearing conditions.

Conclusions

In this study, catfish bones and non-separated animal bones-derived HAp has been produced and a comparison of the physico-mechanical properties has been reported. Therefore, the following conclusions can be reached:

1. From the phase analysis of the produced hydroxyapatites, a dominant phase of HAp was observed with reflections of tetra-calcium phosphate, which is also a biocompatible phase.
2. The higher porosity of prepared catfish bones-derived hydroxyapatite as compared to the non-separated animal bones-derived hydroxyapatite (Table 2) can be useful for applications in biomedicine
3. The hardness values of the synthesized hydroxyapatites are in the range of human cortical bone.
4. The specific mechanical properties of the samples were related to the calculated apparent densities of the samples with the compressive strength increasing from approximately 0.47 to 1.92 MPa for non-separated animal bones-derived hydroxyapatite and catfish bones-derived hydroxyapatite, respectively. This advances the viability of catfish bones-derived hydroxyapatite in this regard for use in biomedical applications where compressive stresses are a common phenomenon.

CRediT authorship contribution statement

E.S. Akpan: Formal analysis, Writing - original draft. **M. Dauda:** . **L.S. Kuburi:** Writing - review & editing. **D.O. Obada:** Formal analysis, Writing - original draft, Writing - review & editing. **D. Dodoo-Arhin:** Writing - original draft, Writing - review & editing.

Declaration of Competing Interest

The authors declare that they have no known competing financial interests or personal relationships that could have appeared to influence the work reported in this paper.

References

[1] Obada DO, Dauda ET, Abifarin JK, Dodoo-Arhin D, Bansod ND. Mechanical properties of natural hydroxyapatite using low cold compaction pressure: Effect of sintering temperature. Mater Chem Phys 2019:122099.
[2] Piccirillo C, Silva MF, Pullar RC, Da Cruz IB, Jorge R, Pintado MME, et al. Extraction and characterisation of apatite-and tricalcium phosphate-based materials from cod fish bones. Mater Sci Eng C 2013;33(1):103–10.
[3] Manjubala I, Sivakumar M, Sampathkumar TS, Panduranga Rao K. Synthesis and characterization of functional gradient materials using Indian corals. J Mater Sci – Mater Med 2000;11(11):705–9.
[4] Rivera EM, Araiza M, Brostow W, Castano VM, Dıaz-Estrada JR, Hernández R, et al. Synthesis of hydroxyapatite from eggshells. Mater Lett 1999;41(3):128–34.
[5] Krishna DSR, Siddharthan A, Seshadri SK, Kumar TS. A novel route for synthesis of nanocrystalline hydroxyapatite from eggshell waste. J Mater Sci – Mater Med 2007;18(9):1735–43.
[6] Dupoirieux L, Neves M, Pourquier D. Comparison of pericranium and eggshell as space fillers used in combination with guided bone regeneration: an experimental study. J Oral Maxillofac Surg 2000;58(1):40–6.
[7] Sakka S, Bouaziz J, Ayed FB. Mechanical properties of biomaterials based on calcium phosphates and bioinert oxides for applications in biomedicine. Adv Biomat Sci Biomed Appl 2013:23–50.
[8] Liu HS, Chin TS, Lai LS, Chiu SY, Chung KH, Chang CS, et al. Hydroxyapatite synthesized by a simplified hydrothermal method. Ceram Int 1997;23(1):19–25.
[9] Hench LL. Bioceramics. J Am Ceram Soc 1998;81(7):1705–28. https://doi.org/10.

1111/j.1151-2916.1998.tb02540.x.
[10] Best SM, Porter AE, Thian ES, Huang J. Bioceramics: past, present and for the future. J Eur Ceram Soc 2008;28(7):1319–27.
[11] Rodriguez-Lorenzo LM, Vallet-Regí M, Ferreira JMF, Ginebra MP, Aparicio C, Planell JA. Hydroxyapatite ceramic bodies with tailored mechanical properties for different applications. J Biomed Mater Res 2002;60(1):159–66.
[12] Akao M, Aoki H, Kato K. Mechanical properties of sintered hydroxyapatite for prosthetic applications. J Mater Sci 1981;16(3):809–12.
[13] Suchanek W, Yoshimura M. Processing and properties of hydroxyapatite-based biomaterials for use as hard tissue replacement implants. J Mater Res 1998;13(1):94–117.
[14] Mezahi FZ, Oudadesse H, Harabi A, Le Gal Y. Effect of ZrO_2, TiO_2, and Al_2O_3 additions on process and kinetics of bonelike apatite formation on sintered natural hydroxyapatite surfaces. Int J Appl Ceram Technol 2012;9(3):529–40.
[15] Gopi D, Shinyjoy E, Sekar M, Surendiran M, Kavitha L, Kumar TS. Development of carbon nanotubes reinforced hydroxyapatite composite coatings on titanium by electrodeposition method. Corros Sci 2013;73:321–30.
[16] Baradaran S, Moghaddam E, Basirun WJ, Mehrali M, Sookhakian M, Hamdi M, et al. Mechanical properties and biomedical applications of a nanotube hydroxyapatite-reduced graphene oxide composite. Carbon 2014;69:32–45.
[17] Heidari F, Razavi M, Bahrololoom ME, Yazdimamaghani M, Tahriri M, Kotturi H, et al. Evaluation of the mechanical properties, in vitro biodegradability and cytocompatibility of natural chitosan/hydroxyapatite/nano-Fe3O4 composite. Ceram Int 2018;44(1):275–81.
[18] Vu MB, Nguyen-Sy T. On the effective anisotropic elastic properties of porous hydroxyapatite, porous collagen, and cortical bone: a homogenization scheme with percolation threshold concept. Mathemat Mechan Solids 2019;24(4):1091–102.
[19] Ramesh S, Tan CY, Bhaduri SB, Teng WD. Rapid densification of nanocrystalline hydroxyapatite for biomedical applications. Ceram Int 2007;33(7):1363–7.
[20] Abifarin JK, Obada DO, Dauda ET, Dodoo-Arhin D. Experimental data on the characterization of hydroxyapatite synthesized from biowastes. Data Brief 2019;26:104485.
[21] Liu K, Sun H, Shi Y, Liu J, Zhang S, Huang S, et al. Research on selective laser sintering of Kaolin–epoxy resin ceramic powders combined with cold isostatic pressing and sintering. Ceram Int 2016;42(9):10711–8.
[22] Dey S, Das M, Balla VK. Effect of hydroxyapatite particle size, morphology and crystallinity on proliferation of colon cancer HCT116 cells. Mater Sci Eng C 2014;39:336–9.
[23] Ayed FB, Bouaziz J, Bouzouita K. Calcination and sintering of fluorapatite under argon atmosphere. J Alloy Compd 2001;322(1–2):238–45.
[24] Landi E, Tampieri A, Celotti G, Sprio S. Densification behaviour and mechanisms of synthetic hydroxyapatites. J Eur Ceram Soc 2000;20(14–15):2377–87.
[25] Munar ML, Udoh KI, Ishikawa K, Matsuya S, Nakagawa M. Effects of sintering temperature over 1,300 C on the physical and compositional properties of porous hydroxyapatite foam. Dent Mater J 2006;25(1):51–8.
[26] Medellin-Castillo NA, Leyva-Ramos R, Padilla-Ortega E, Perez RO, Flores-Cano JV, Berber-Mendoza MS. Adsorption capacity of bone char for removing fluoride from water solution. Role of hydroxyapatite content, adsorption mechanism and competing anions. J Ind Eng Chem 2014;20(6):4014–21.
[27] Barakat NA, Khil MS, Omran AM, Sheikh FA, Kim HY. Extraction of pure natural hydroxyapatite from the bovine bones bio waste by three different methods. J Mater Process Technol 2009;209(7):3408–15.
[28] Alpat SK, Özbayrak Ö, Alpat Ş, Akçay H. The adsorption kinetics and removal of cationic dye, Toluidine Blue O, from aqueous solution with Turkish zeolite. J Hazard Mater 2008;151(1):213–20.
[29] Boutinguiza M, Pou J, Comesaña R, Lusquiños F, De Carlos A, León B. Biological hydroxyapatite obtained from fish bones. Mater Sci Eng C 2012;32(3):478–86.
[30] Ivankovic H, Ferrer GG, Tkalcec E, Orlic S, Ivankovic M. Preparation of highly porous hydroxyapatite from cuttlefish bone. J Mater Sci – Mater Med 2009;20(5):1039–46.
[31] Akram M, Ahmed R, Shakir I, Ibrahim WAW, Hussain R. Extracting hydroxyapatite and its precursors from natural resources. J Mater Sci 2014;49(4):1461–75.
[32] Yoganand CP, Selvarajan V, Cannillo V, Sola A, Roumeli E, Goudouri OM, et al. Characterization and in vitro-bioactivity of natural hydroxyapatite based bioglass–ceramics synthesized by thermal plasma processing. Ceram Int 2010;36(6):1757–66.
[33] Huang YC, Hsiao PC, Chai HJ. Hydroxyapatite extracted from fish scale: Effects on MG63 osteoblast-like cells. Ceram Int 2011;37(6):1825–31.
[34] Chang HH, Cheng CL, Huang PJ, Lin SY. Application of scanning electron microscopy and X-ray microanalysis: FE-SEM, ESEM-EDS, and EDS mapping for studying the characteristics of topographical microstructure and elemental mapping of human cardiac calcified deposition. Anal Bioanal Chem 2014;406(1):359–66.
[35] Karageorgiou V, Kaplan D. Porosity of 3D biomaterial scaffolds and osteogenesis. Biomaterials 2005;26(27):5474–91.
[36] Mirzaali MJ, Schwiedrzik JJ, Thaiwichai S, Best JP, Michler J, Zysset PK, et al. Mechanical properties of cortical bone and their relationships with age, gender, composition and microindentation properties in the elderly. Bone 2016;93:196–211.
[37] Vuola J, Taurio R, Göransson H, Asko-Seljavaara S. Compressive strength of calcium carbonate and hydroxyapatite implants after bone-marrow-induced osteogenesis. Biomaterials 1998;19(1–3):223–7.
[38] Kobayashi S, Kawai W, Wakayama S. The effect of pressure during sintering on the strength and the fracture toughness of hydroxyapatite ceramics. J Mater Sci – Mater Med 2006;17(11):1089–93.
[39] Goller G, Oktar FN, Agathopoulos S, Tulyaganov DU, Ferreira JMF, Kayali ES, et al. Effect of sintering temperature on mechanical and microstructural properties of bovine hydroxyapatite (BHA). J Sol-Gel Sci Technol 2006;37(2):111–5.
[40] Yazdanpanah Z, Bahrololoom ME, Hashemi B. Evaluating morphology and mechanical properties of glass-reinforced natural hydroxyapatite composites. J Mech Behav Biomed Mater 2015;41:36–42.
[41] Pal A, Paul S, Choudhury AR, Balla VK, Das M, Sinha A. Synthesis of hydroxyapatite from Lates calcarifer fish bone for biomedical applications. Mater Lett 2017;203:89–92.
[42] Ramesh S, Natasha AN, Tan CY, Bang LT, Ching CY, Chandran H. Direct conversion of eggshell to hydroxyapatite ceramic by a sintering method. Ceram Int 2016;42(6):7824–9.
[43] Kumar GS, Thamizhavel A, Girija EK. Microwave conversion of eggshells into flower-like hydroxyapatite nanostructure for biomedical applications. Mater Lett 2012;76:198–200.
[44] Pramanik S, Agarwal AK, Rai KN, Garg A. Development of high strength hydroxyapatite by solid-state-sintering process. Ceram Int 2007;33(3):419–26.
[45] Kamalanathan P, Ramesh S, Bang LT, Niakan A, Tan CY, Purbolaksono J, et al. Synthesis and sintering of hydroxyapatite derived from eggshells as a calcium precursor. Ceram Int 2014;40(10):16349–59.
[46] Gergely G, Wéber F, Lukács I, Tóth AL, Horváth ZE, Mihály J, et al. Preparation and characterization of hydroxyapatite from eggshell. Ceram Int 2010;36(2):803–6.
[47] Boanini E, Gazzano M, Bigi A. Ionic substitutions in calcium phosphates synthesized at low temperature. Acta Biomater 2010;6(6):1882–94.
[48] Wang J, Shaw LL. Nanocrystalline hydroxyapatite with simultaneous enhancements in hardness and toughness. Biomaterials 2009;30(34):6565–72.
[49] Wu SC, Hsu HC, Hsu SK, Chang YC, Ho WF. Effects of heat treatment on the synthesis of hydroxyapatite from eggshell powders. Ceram Int 2015;41(9):10718–24.
[50] Koutsopoulos S. Synthesis and characterization of hydroxyapatite crystals: a review study on the analytical methods. J Biomed Mater Res 2002;62(4):600–12.
[51] Aminzare M, Eskandari A, Baroonian MH, Berenov A, Hesabi ZR, Taheri M, et al. Hydroxyapatite nanocomposites: synthesis, sintering and mechanical properties. Ceram Int 2013;39(3):2197–206.
[52] Slosarczyk A, Białoskórski J. Hardness and fracture toughness of dense calcium–-phosphate-based materials. J Mater Sci - Mater Med 1998;9(2):103–8.
[53] Yeong KCB, Wang J, Ng SC. Mechanochemical synthesis of nanocrystalline hydroxyapatite from CaO and CaHPO4. Biomaterials 2001;22(20):2705–12.
[54] Lin K, Chen L, Chang J. Fabrication of dense hydroxyapatite nanobioceramics with enhanced mechanical properties via two-step sintering process. Int J Appl Ceram Technol 2012;9(3):479–85.
[55] Song J, Liu Y, Zhang Y, Jiao L. Mechanical properties of hydroxyapatite ceramics sintered from powders with different morphologies. Mater Sci Eng A 2011;528(16–17):5421–7.
[56] Ruys AJ, Sorrell CC. Hydroxyapatite sintering characteristics: correlation with powder morphology by high-resolution microscopy. J Mater Sci Lett 1995;14(10):744–7.
[57] Rhee SH. Synthesis of hydroxyapatite via mechanochemical treatment. Biomaterials 2002;23(4):1147–52.